Controlling Particle Dispersion in a Transverse Jet by Synchronized Injection

Marina Campolo and Andrea Cremese
Centro Interdipartimentale di Fluidodinamica e Idraulica, Dipartimento di Energetica e Macchine, Università degli Studi di Udine, Via delle Scienze 208, 33100 Udine, Italy

Alfredo Soldati
Centro Interdipartimentale di Fluidodinamica e Idraulica, Dipartimento di Energetica e Macchine, Università degli Studi di Udine, Via delle Scienze 208, 33100 Udine, Italy and
Dept. of Fluid Mechanics, CISM, 33100 Udine, Italy

DOI 10.1002/aic.11536
Published online June 10, 2008 in Wiley InterScience (www.interscience.wiley.com).

The dispersion produced by a jet injecting microparticles (or droplets) in a cross stream is controlled by the interaction between injected species and large scale flow structures characteristic of the jet in crossflow system. In a previous work we characterized accurately the dynamics of the particles undergoing dispersion under the action of the shear layer vortices (SLV) which form in the jet shear layer. In this article, we propose a strategy to control and possibly optimize the dispersion of species injected in the cross stream. This strategy is based on injecting particle packets (or puffs) synchronized with the time of formation of the shear layer vortices. The possibility to increase or decrease particle dispersion by synchronized, pulsed injection is explored by identifying the relevant parameters of the particle/flow system; the effectiveness of this strategy is verified by exploring a representative sample of the parameter range.
© 2008 American Institute of Chemical Engineers *AIChE J,* 54: 1975–1986, 2008
Keywords: transverse jet, dispersion, segregation, microparticles, pulsed injection

Introduction

Fuel injection in combustion chambers, postcombustion control devices (such as transverse injection of ammonia solution for NO_x abatement), hot gas quenching with sprays, spray dryers, and spray coating systems are but a few examples of industrial flow configurations in which the crucial task is to achieve effective mixing between a dispersed phase (particles or droplets) and a main stream. In most of these applications, species are injected by a carrier fluid normal to the main, transverse stream. This configuration—that is, the transverse jet or the jet in crossflow—is indeed very effective in dispersing the species: the jet flow and the crossflow can be tuned to obtain the desired mixing effect some distance away from the jet exit. In some applications related to reacting flows, even more strict control of species dispersion is required to avoid, also in the injection region, the formation of zones where the high/low concentration of species can be detrimental to the process (for instance, generating a reduced thermal efficiency in combustion applications or a reduced abatement efficiency in systems designed for pollution control). Such a degree of control requires a deep understanding of the mixing dynamics of the transverse jet and the identification of the parameters relevant to dispersion control which can be exploited to set up "ad-hoc" control strategies. The aim of the present work is to make a step in this direction. Specifically, we want to investigate how the injection process

Correspondence concerning this article should be addressed to M. Campolo at marina.campolo@uniud.it.
Current address of A. Cremese: Arup Group, London, UK.
Current address of A. Soldati: EPFL, Lausanne, Switzerland.

© 2008 American Institute of Chemical Engineers

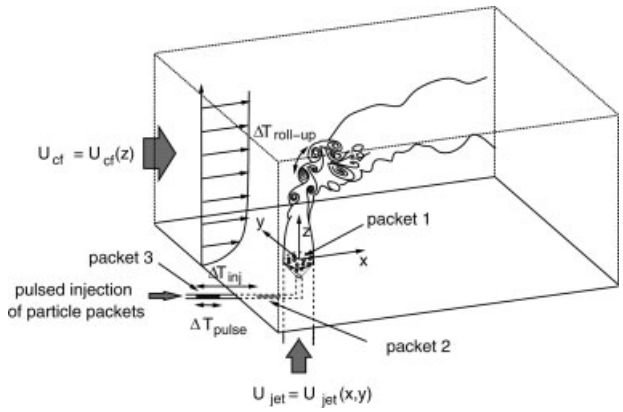

Figure 1. Sketch of the problem domain and of the strategy proposed to control interphase mixing by pulsed injection of particles.

can be optimized considering the time dependent nature of the structures controlling mixing in the transverse jet.

A typical configuration of a jet in crossflow is shown in Figure 1. The flow field generated by the jet, drawn based on the experimental pictures presented by Lim et al.[1] is characterized by the instability of the jet shear layer which, even under steady state conditions (i.e., constant velocity profile for the jet and the transverse stream), promotes the (quasi periodical) formation of large-scale roll-up structures (shear layer vortices, SLVs) at the jet interface.

The structure of the flow field is characterized by a number of different scales[2] interacting in a complex way which is still under serious investigation.[3–8] However, in our previous work,[9] we have observed that of all the flow structures the shear layer vortices are those controlling transport and dispersion of the particles issued by the jet.

Considering the many engineering and environmental applications in which the jet in crossflow system is used, we believe that a strategy to enhance/reduce mixing of injected species or particles would be mostly desirable. A number of experimental and numerical analyses ([9–11]among others) have shown that the interaction between injected droplets/particles and fluid structures is crucial to enhance penetration, promote dispersion, and obtain a satisfactory degree of interphase mixing. This interaction is most effective when the particle response time, which scales with particle density and squared diameter and is inversely proportional to fluid viscosity, is comparable with the relevant fluid time scale.[9] However, even if this criterion is met, a homogeneous particle distribution is not necessarily obtained.[12] We acknowledge here that homogeneous distribution of dispersed species may be an unreachable object; yet, we would be satisfied if we could identify a suitable strategy to "maximize" or "minimize" particle dispersion: in other words, a control strategy.

As shown by several experimental studies (see Refs. 13, 14 among others), jet forcing may be a simple way to control the generation of large-scale mixing structures in the transverse jet and thus to improve the dispersion of species. It is our opinion that the same kind of control can be achieved without forcing the jet, through a pulsed injection of particles and the precise synchronization between particle injection and flow structures dynamics.

To ground firmly this claim, we perform numerically the experiment sketched in Figure 1. Specifically, we seed discontinuously the (steady state) jet with droplets and follow their dispersion. Since we want to prove a "concept" strategy able to control particle dispersion, we rely on a prototypical, simple simulation methodology to identify the fundamental parameters to monitor to achieve particle dispersion control. We should remark here that, in this article, we are not concerned with the close simulation of the real phenomenon; our simulation aims at reproducing only the fundamental characteristics of the transverse jet which have effects on particle dispersion, that is, the interaction between the jet and the crossflow boundary layer and the interaction between particles and vortical structures. A more complex simulation could perhaps be closer to the physical phenomenon, and yet could definitely make more difficult the identification of the mixing control strategy. For our analysis, we assume that the flow is diluted, particles are monodispersed and particle–particle interaction and wall–particle interaction can be neglected. Therefore, the words *droplets* and *particles* will be used interchangeably to indicate the dispersed phase, considering that the behavior of particles and droplets is the same in these conditions. In a real injection system, particle–particle collisions will be an important issue in the regions where the particle concentration is large, that is, typically in the issuing pipe and in the near field of the jet. In the case of droplets, particle–particle collisions will determine also the size distribution of droplet diameters at the jet exit. It is beyond the purpose of this article to simulate such complex phenomena. However, we expect that the relevant parameters identified to control the dispersion of monodispersed, noninteracting, rigid particles will be the same controlling also the dispersion of poly dispersed, colliding particles.

Figure 1 shows three groups of particles: a group of particles (packet 1) right at the jet exit and two subsequent groups of particles (packets 2 and 3, respectively) ready for injection. Protocols for pulsed particle injection can be described by two main temporal parameters: (i) the first is the finite time, ΔT_{pulse}, during which particles are injected; (ii) the second is the time period between the injection of subsequent particle packets, ΔT_{inj}. The particle injection cycle is thus based (see Figure 1) on the time period ΔT_{inj}; within each cycle, an active period called ΔT_{pulse} is started during which particle injection is on, followed by an inactive period lasting $\Delta T_{\text{inj}} - \Delta T_{\text{pulse}}$ during which particle injection is off. To control interphase dispersion, ΔT_{pulse} and ΔT_{inj} should be chosen accordingly to the period of formation of the structures (SLVs) which control particle transport in the transverse stream, $\Delta T_{\text{roll-up}}$. The objects of this work are thus (i) to characterize ΔT_{inj}; (ii) to characterize ΔT_{pulse}, and (iii) to establish when the particle cycle should start *with reference to a relevant time which describes the dynamics of the jet in crossflow system*. We acknowledge that the investigated system is just a demo; yet, it retains all the significant features of the industrial system we want to investigate and is thus a perfect tool to verify our strategy which could be then quantitatively framed in any of the specific applications.

Based on the scaling arguments presented in Ref. 9, it is straightforward to assume that ΔT_{inj} should scale with the periodicity of the shear layer vortices formation, which we defined as $\Delta T_{\text{roll-up}}$. We will also restrict our analysis to a

range of ΔT_{pulse} which is much shorter than ΔT_{inj}. A critical issue will thus be to characterize when the ΔT_{inj} cycle should start. The problem is not trivial because of the following reasons. For practical arguments, we decided to study a system in which particles are injected at the jet mouth. However, the SLVs which control particle dispersion will form several diameters downstream the jet mouth, in a location not fixed in space.[2] This location can be extremely sensitive (i) to the jet velocity profile at the jet mouth, which in turn depends on the coupling between the jet and the crossflow which may extend its influence even deep within the pipe, and (ii) to the turbulence intensity, both in the jet and in the crossflow. Whichever the initial location of the generated vortices, to maximize entrainment of particles by SLVs a precise synchronization between particles injected at the jet mouth and SLVs formed away from the jet mouth is crucial. Considering also that particles will not necessarily travel at the same speed of the flow perturbation which is generated at the jet mouth and which produces the SLVs, we made a number of experiments trying to correlate the beginning of the particle cycle with a relevant flow property measured near to the jet mouth.

In our model of the jet in crossflow, we neglect (i) the effect of turbulence, both in the issuing jet and in the crossflow, (ii) the coupling between the jet and the crossflow inside the nozzle, and (iii) the precise velocity profile at the jet exit. The jet is thus simulated imposing an axial symmetric, steady state velocity profile right at the jet mouth.

We thus compared qualitatively the dispersion patterns obtained in this flow for different delay of injection and we introduced *ad-hoc* measures to quantify the dispersion and preferential segregation of particles, that is, the extent and homogeneity of interphase mixing. Our final object is to evaluate if interphase dispersion can be controlled (promoted/forbidden) by tuning the delay of injection. In this case, synchronized pulsed injection of species could be adopted as a very simple way to control mixing in many industrial applications, like combustion and pollution control.

The article is organized as follows. First, we present the problem geometry and the numerical methodology and we characterize briefly the fluid dynamics of transverse jets (see, for instance, Refs. 2 and 15) and their time dependent evolution.[2,16] Second, we describe the strategy adopted to evaluate the effect of injection synchronization on particle behavior. In the results section, we describe qualitative differences in particle dispersion patterns and we introduce quantitative measures of particle dispersion and segregation. Finally, we summarize the potentials of the strategy for mixing control.

Methodology

Computational domain and numerical simulation

In our numerical experiment, we consider an upward jet of air (density $\rho = 1.4$ kg/m^3 and viscosity $\upsilon = 1.29 \times 10^{-5}$ m^2/s) injecting water droplets (density $\rho_p = 1000$ kg/m^3) into a cross stream of air. Computational domain and boundary conditions for the problem are sketched in Figure 1. The reference coordinate system is centered at the jet exit. Here, the jet exit diameter, $D = 0.01$ m, is used as reference length scale. The computational domain (dotted box in Figure 1) extends from $-3 \div 9$ D in the streamwise, $-4 \div 4$ D in the spanwise and $0 \div 9$ D in the vertical direction (x, y, and z coordinates, respectively). The dimensions of the computational domain are reduced to the minimum necessary since we focus our analysis on the near field of the jet, where dispersion control is most difficult to achieve.

The jet enters the box from a circular orifice in the bottom wall (mean velocity $U_{jet} = 2.57$ m/s). Its velocity profile corresponds to a steady state, analytic, axi-symmetric pipe flow. The crossflow enters the box from the plane $x = -3$D (unperturbed velocity $U_{cf} = 0.514$ m/s). Its velocity profile corresponds to a steady state, laminar boundary layer (thickness $\delta = 0.5$D). Top side, lateral sides, and outlet side of the box are open for the flow (free slip surfaces and outlet section, respectively). The jet Reynolds number and the crossflow Reynolds number based on fluid properties and jet exit diameter are $Re_{jet} = U_{jet}D/\upsilon = 2000$ and $Re_{cf} = U_{cf}D/\upsilon = 400$, respectively. The jet-to-crossflow velocity ratio, α, is 5.

In this work, we are not specifically concerned with the conditions chosen for the analysis. We preferred to refer to the natural jet to avoid any loss of generality: periodic or quasi periodic formation of shear layer vortices can originate from natural shear instability, from jet pulsation or from crossflow pulsation (see, for instance, Ref. 17). The results we will show are thus valid for the unforced jet and for the forced jet as a particular case. The choice to simulate the flow in these specific conditions was driven by the following considerations: (i) according to[2] values of Re_{jet}, Re_{cf}, and α are in the range for which quasi periodic formation of shear layer vortices has been observed experimentally; (ii) the jet Reynolds number is small, and fluctuations of velocity in the pipe issuing the jet and the particles can be neglected.

We are aware that the evolution of transverse jets is extremely sensitive to the jet velocity profile. In principle, the velocity profile imposed at the jet boundary to simulate numerically the issuing jet should reproduce carefully three kinds of effects: (i) the development of the flow along the issuing pipe; (ii) the coupling between the transverse flow and the flow within the pipe; (iii) the level of turbulence of the issuing jet. We have investigated to some extent the complexity of the problem, in Ref. 8. In Ref. 8, we evaluated the coupling between the transverse flow and the flow within the pipe calculating the variation of the flow field inside the pipe when the transverse flow is switched off (jet issued in quiescent fluid) and when the transverse flow is switched on. We found (see Figure 4 in Ref. 8) that for $\alpha < 20$ is always necessary to simulate a segment of pipe upstream the jet exit to account for the variation of the velocity profile in the pipe section (with respect to a pipe flow producing a free jet). Yet, we found (see Figure 6 of the same article) that these variations have little effect for the evaluation of the jet trajectory when $\alpha \geq 5$. Therefore, in this work, we chose to neglect the coupling between the crossflow and the jet inside the pipe, we do not simulate the pipe/plenum, and we impose a velocity profile for the jet right at the jet mouth.

As shown by Ref. 7 in Figure 9 of their article, the time averaged velocity profile at the jet exit does not change significantly before the jet exit for large enough α (profiles of mean axial velocity shown 2D and 1D upstream the jet exit do not differ much from the profile at the jet exit for $\alpha = 5.7$). Therefore, as far as a time averaged velocity profile is used as boundary condition at the jet inlet, the velocity pro-

file can be considered symmetric and similar to the one calculated some distance inside the jet exit. We are aware that, if the inlet turbulence is properly accounted for in the simulation, modifications in the turbulence budget terms along the issuing pipe (as shown by Ref. 7 in their Figure 14) may affect the development of the flow in the transverse jet. However, neglecting the effect of turbulence in our model of the jet will have no affect in the identification of the strategy for particle dispersion control. Different conditions will affect *the values* of the parameters identified for particle dispersion control but will not modify the choice of *the relevant parameters*.

We solve for the flow using the finite volume solver previously described in Ref. 18. The grid is nonuniform and made of $92 \times 58 \times 51$ finite volumes. Smaller volumes are used to describe precisely the flow in the jet exit region. The minimum grid resolutions are $\Delta x = 0.000260$, $\Delta y = 0.000552$, and $\Delta z = 0.000264$, that is, 0.86, 1.83, and 0.86 times the shear layer thickness at the jet exit, which is here considered as the relevant length scale for the mixing layer. This resolution is sufficient to capture the evolution of the shear layer vortices[9] which are described by at least nine grid points from the early stages of their formation.

Finite volume solver

For the incompressible flow considered here, the governing equations are Navier-Stokes and continuity equations (omitted here for sake of brevity). The governing equations are discretized on a colocated grid using a finite volume approach, following the technique proposed in Ref. 19. The reader is referred to the articles in Refs. 9 and 18 for further details.

We calculated the flow field evolution starting from the condition of still fluid up to statistical convergence (about four times the through-flow period, $T_{ctf} = 12D/U_{cf} = 0.233$ s, corresponding to 200 t_u, where the time unit t_u is defined as $t_u = D/U_{jet} = 3.89 \times 10^{-3}$ s). Then, we calculated the flow field evolution for a time period of 450 time units (about 6.6 times the through-flow period) to compute the flow field statistics.

Lagrangian tracking

We chose to analyze particle dispersion over a time window spanning one channel through-flow. We start the injection of droplets when the flow field is fully developed. Droplets are injected as subsequent non overlapping packets (490 packets for all simulations), each made of 5000 water droplets. For each packet, the pulsed injection duration is set equal to $\Delta T_{pulse} = 0.48 \times 10^{-3}$ s. Since the time period of vortex shedding is $\Delta T_{roll\text{-}up} = 0.019$ s (see Ref. 9), during the simulated time window, about 12 shear layer vortices form at the jet tip, grow up in the jet shear layer and eventually decay in the body of the jet. As mentioned, in this work, the particle injection cycle, ΔT_{inj}, is taken equal to the periodicity of the shear layer vortices formation, $\Delta T_{roll\text{-}up}$; therefore, 40 subsequent particle packets are injected during each vortex shedding period. Injection times of these 40 packets cover all the possible delays between the particle injection time and the time of formation of one SLV, even if the precise time at which the SLV forms is unknown.

We chose to simulate particle diameters equal to 5, 10, and 50 μm. The dimensionless characteristic time, $\tau_p^+ = (\rho_p {D_p}^2/18\mu)/t_u$, varies from 1.97×10^{-2} to 1.97. According to the time scaling we propose in Ref. 9, which is based on the time of circulation of shear layer vortices, $T_{slv} = 1.2 \times 10^{-4}$ s, that is, the structures controlling mixing, Stokes (St* $= \tau_p/T_{slv}$) are 0.64, 2.56, and 64, respectively. These values identify particles which are responsive (5 μm and 10 μm) and less responsive (100 μm) to the mixing vortices. Five micrometer particles will be specifically considered in the analysis of results, since their Stokes Number is closest to unity, that is, their characteristic time is the most similar to the relevant fluid time scale and the maximum interaction between particles and structures is expected.

We calculate the trajectory of each particle by integrating explicitly over time the equation of motion. The assumptions for particle modeling are as follows: (i) all particles are noninteracting, nondeformable solid spheres; (ii) particle density is large compared with fluid density; (iii) the effect of the particles on the flow is neglected; (iv) virtual mass, pressure gradient, and Basset forces are neglected (see Ref. 9). For the specific flow system examined here, neglected terms have a limited effect since the droplet Stokes number St* $= \tau_p/T_{slv}$ is in the range $[0.64 \div 64]$.[9] The equation of motion reduces to a balance of Stokes drag, buoyancy forces and particle inertia, as reported in Ref. 9 and has the following form:

$$\rho_p \frac{\pi D_p^3}{6} \frac{d\vec{\mathbf{v}}_p}{dt} = \frac{1}{2} C_D \frac{\pi D_p^2}{4} \rho(\vec{\mathbf{v}} - \vec{\mathbf{v}}_p)\left|\vec{\mathbf{v}} - \vec{\mathbf{v}}_p\right| + \frac{\pi D_p^3}{6}(\rho_p - \rho)\vec{\mathbf{g}} \tag{1}$$

where ρ_p, D_p, and $\mathbf{v_p}$ are particle density, diameter, and velocity, ρ and $\mathbf{v}$ are fluid density and velocity, t is time, and $\mathbf{g}$ is gravity. The Stokes coefficient for drag, $C_D = f(\mathrm{Re}_p)$, is given by[20]:

$$C_D(\mathrm{Re}_p) = \frac{24}{\mathrm{Re}_p}(1 + 0.15 \cdot \mathrm{Re}_p^{0.687}) \tag{2}$$

where $\mathrm{Re}_p = \rho\, D_p\, |\mathbf{v} - \mathbf{v_p}|/\mu$ is the particle Reynolds number and μ is the fluid viscosity. The drag force is evaluated by calculating the fluid velocity, $\mathbf{v}$, at each particle position using trilinear interpolation of velocity values at cell centers.

The initial velocity of particles, released at the jet exit, is set equal to the local fluid velocity. The assumption of local equilibrium between particles and fluid at the jet exit may appear to be over simplistic. Yet, it represents a reasonable choice until a more detailed characterization of the dispersed phase at the jet exit is not available. In a more complex simulation, closer to the physical phenomenon, the behavior of particles and droplets may be influenced by the specific injection system, by particle–particle interaction and by the local level of turbulence of the issuing stream. The investigation of these effects in beyond the purpose of the present article. However, specific inlet conditions for the dispersed phase are expected to have no effect on the qualitative behavior of the particle/flow system, introducing only quantitative variations on results.

The equation of motion is integrated with an explicit Runge-Kutta fourth order method using an integration time

Table 1. Summary of CPU Times

Simulation Step	Simulated Time [T_{ctf}]	Δt	CPU time
Flow field development	4 (+6.6)	7.5×10^{-5} s	20 h
Flow field for particle tracking	1	3×10^{-5} s	5 h
Particle tracking (one D_p)	1	3×10^{-5} s	90 h

T_{ctf} = channel through-flow period

step equal to 3×10^{-5} s, that is, one half of the characteristic time of the smallest particle, $\tau_{p\ 5\ \mu m}$, as in Ref. 21.

Computational cost

Calculations have been performed on a HP workstation xw4200 (3.8 GHz CPU, 2 Gb RAM) in three steps: (i) calculation of fully developed flow field and statistics, (ii) calculation of flow field for particle tracking, (iii) Lagrangian tracking of particle packets. The computational costs are summarized in Table 1.

Results

Characterization of shear layer vortices

The behavior of the particle/flow system is controlled (i) by the periodic evolution of the shear layer vortices; (ii) by the probability that particles are where the SLVs can entrain them; (iii) by the mutual interaction occurring between the single particle (or the particle cluster) and the SLVs (controlled by the Stokes number). Therefore, knowing precisely the characteristics of the SLVs as mixing agents is necessary to identify possibly optimized injection protocols.

Shear layer vortices are shed at characteristic Strouhal frequencies[15] and dominate the initial portion of the jet. As discussed in Refs. 22–24 for free jets, and in Refs. 2 and 25 for transverse jet, SLVs form some distance downstream the jet exit. It is beyond the scope of this article to describe the mechanisms which form the vortices. It will be sufficient here to precise that the formation of the SLVs is linked to fluctuations in the pressure, velocity, and vorticity fields. These fluctuations, which can be detected by probes, contain information on the frequency of formation of SLVs and on their characteristic advection time scale. In experiments (see for instance Ref. 26), the frequency of formation of SLVs is measured at the position of the monitoring probe where the amplitude of signal variation is maximum. Interestingly, signal fluctuations may be detected even at the jet exit, where the SLVs are not-yet-formed, giving a chance to "predict" the incipient formation of SLVs which detach some distance away from the jet inlet.[27]

Here, our aim is to characterize the SLVs to (i) synchronize the pulsed injection of particles with the frequency of formation of SLVs and to (ii) optimize the time-shift of particle injection to maximize their interaction with the not-yet-formed SLVs. We considered 12 monitoring points positioned along the upper shear layer of the jet, as shown in Figure 2, sampling over time the spanwise vorticity signal. The coordinates of each sensor are reported in Table 2. We will focus on the four sensors 1, 2, 6, and 8 indicated in

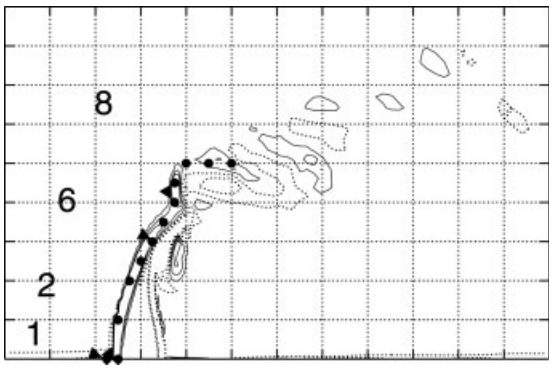

Figure 2. Snapshot of spanwise vorticity, $\omega_y^+ = t_u \times \omega_y$, in the jet symmetry plane and location of sensors used for flow structure characterization.

Sensors are numbered from 1 to 12 from left to right and bottom up. Isocontours are −2.5, −1.5, −0.5 (solid line) and 0.5, 1.5 (dashed line).

Figure 2. Figure 3a shows the variation of the signal sampled at these sensors. Sensor 1 is located slightly upstream the jet exit; sensor 2 is located near the jet exit; sensor 6 is located around the region where the shear layer vortices form; sensor 8 is located around the region where the shear layer vortices detach. For an easier comparison, signals have been normalized using the local mean value and standard deviation of the spanwise vorticity. Figure 3 shows that vorticity signals monitored at different sensor positions are characterized by a slightly different frequency content which may be linked to the local dynamics of SLVs (i.e., formation, merging, and pairing) (see Refs. 25, 27, 28, among others). Results of autocorrelation analysis on spanwise vorticity signals are shown in Figure 3(b). No significant periodicity is observed for the normalized spanwise vorticity, $\omega_{y,N}$, at sensor 1 in the time window [0:0.06 s], and the corresponding auto correlation plot shows no peak. Peaks in the autocorrelation plots are produced at $T_{oscillation,I} = 0.008$ s for sensor 6 and at $T_{oscillation,II} = 0.0165 \div 0.0175$ s for sensors 2, 6, and 8. $T_{oscillation,II}$ is in the range generally associated with the formation of shear layer vortices (shear layer mode). $T_{oscillation,I}$, which is almost one half of $T_{oscillation,II}$, can be associated with higher frequency oscillations at the jet tip. We should remark here that it is rather difficult to measure precisely the frequency for vortex shedding: (i) the frequency of formation of SLVs is present even near to the jet

Table 2. Position of Sensors Along the Jet Shear Layer

Sensor n.	*x/D*	*y/D*	*z/D*
1	0.75	0.	0.001
2	0.52	0.	0.001
3	0.52	0.	1.0
4	0.25	0.	2.0
5	0.	0.	2.5
6	0.25	0.	3.0
7	0.5	0.	3.5
8	0.75	0.	4.0
9	0.75	0.	4.5
10	1.	0.	5.
11	1.5	0.	5.
12	2.	0.	5.

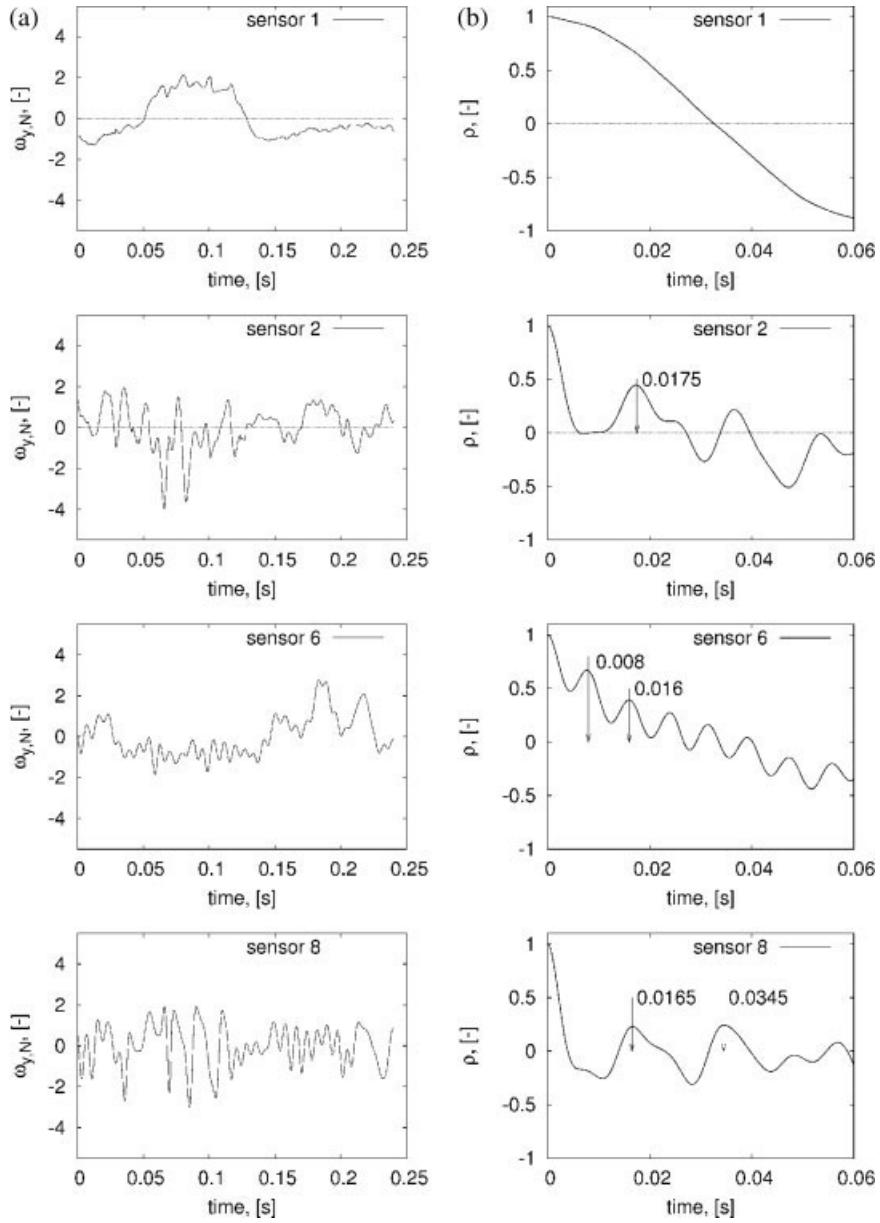

Figure 3. (a) Normalized spanwise vorticity, $\omega_{y,N}$, sampled at different sensor locations. Vorticity values are normalized with respect to local mean value and local standard deviation; (b) correlation analysis of spanwise vorticity signal used to evaluate roll-up period for shear layer vortices.

exit (sensor 2), and yet (ii) the frequency may change slightly if measured at larger distances from the jet exit (for instance, $T_{\text{oscillation,II}} = 0.019$ s at $[x/D,y/D,z/D] = [3,0,6]$).

During their motion, shear layer vortices span the same region of the flow in which particles are moving driven by their initial momentum. Particles entrained by the SLVs can leave their original probable trajectory, being transported into different regions of the flow. To understand the behavior of the particle/flow system, we tried to characterize the shear layer vortices shed at the upper side of the jet (counter clock-wise rotation) considering their trajectory, their advection velocity, and their vorticity. We identified and tracked over time the shear layer vortices by processing several instantaneous fields of spanwise vorticity calculated in the jet symmetry plane with a methodology similar to Ref. 29. As discussed previously, variations of spanwise vorticity are already detected near to the jet exit (sensor 2, in Figure 3), where the SLVs are not-yet-formed. Therefore, we considered a control-window centered at the upstream half of the orifice, right above the jet exit, and monitored over time the values of spanwise vorticity. We identified the core of a new, not-yet-born shear layer vortex from the presence of a significant local minimum of vorticity. When a new shear layer vortex is identified, the control-window is moved in the symmetry plane at the velocity of the fluid in the core of the vortex, and the new position of the minimum of vorticity is

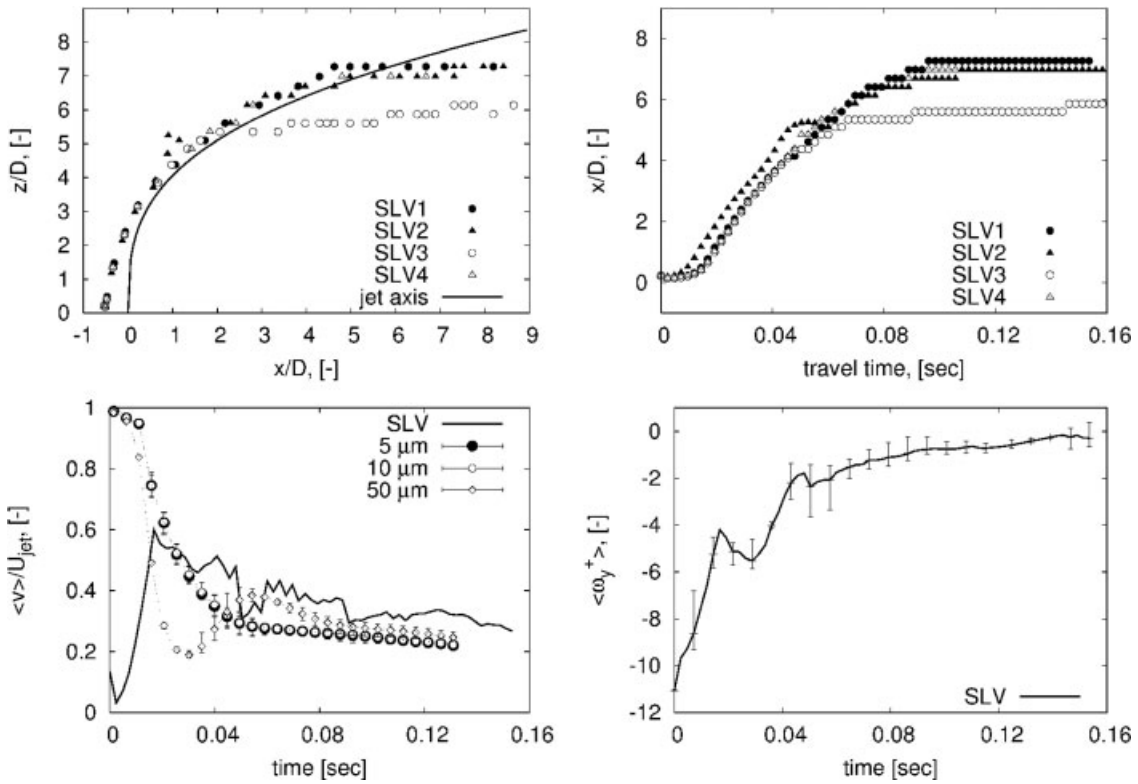

Figure 4. (a) Trajectories of shear layer vortices (SLV) and jet axis (solid line); (b) travel time of shear layer vortices; variation of (c) mean advection velocity associated to shear layer vortices moving downstream along the jet (thick line) and variation of mean velocity of injected particles of different size (errorbars indicate range of variation over different particle packets); (d) dimensionless mean spanwise vorticity, $\omega_y^+ = t_u \times \omega_y$, associated to shear layer vortices moving downstream along the jet (errorbars indicate range of variation over different SLV).

found. The new position of the vortex core is used to describe the trajectory of the shear layer vortex and to calculate its travel time. The displacement over time of the vortex core is used as a measure of the advection velocity of the shear layer vortex and the value of spanwise vorticity calculated at the vortex core is used to represent the spanwise vorticity of the shear layer vortex. As already observed in Ref. 2, we find that the advection velocity estimated from the relative displacement of the vortex core is very similar to the fluid velocity in the core of the SLV.

Values shown in Figures 4a–d have been obtained from the analysis of several (12) SLVs during their travel in the streamwise direction. Figures 4a and b show the trajectory of four representative SLVs and the corresponding time of travel to reach a given position downstream the jet inlet; Figures 4c and d show the variation of the advection velocity and the spanwise vorticity calculated averaging over 12 SLVs. Consider first Figure 4a. In the first part of their travel, SLVs shed at the upstream side of the jet move above the jet axis, defined as the locus of point of maximum velocity and shown as a thick line. Three shear layer vortices (out of the four shown) remain above the jet axis, one is entrained in the body of the jet for $x/D > 3$. Figure 4(b) shows that SLVs moving above the jet axis are advected downstream faster than those entrained in the low velocity region in the body of the jet. SLVs become difficult to track for $x/D > 5$. Figures 4c and d show that, as expected, the advection velocity and spanwise vorticity of SLVs vary widely over the domain (see Ref. 2). Specifically, the velocity increases over time until SLVs detach from the jet tip, and then decreases as SLVs move far away from the jet exit.

To understand the behavior of the particle/flow system, we compared the advection velocity of SLVs and the velocity of packets of particles of different size injected with the jet, as shown in Figure 4(c). At the time of injection, the velocity is the same for all the particle packets and is equal to the jet velocity. We remark here that it is our assumption to prescribe an initial particle velocity equal to the fluid velocity. Other assumptions may change this figure but not the physics underlying our strategy. After injection, the decrease of velocity depends on particle diameter: velocity decreases faster for 50 μm particles which penetrate deeper above the jet. Comparing the variations over time of the velocities calculated for particles and shear layer vortices, it is clear that, at least in the first stages of injection, (most of) the particles move faster than the SLVs. This means that their motion is decoupled from the fluid and that they are unable to interact with SLVs. Particle velocity and velocity of shear layer vortices become comparable (i.e., effective coupling is possible) after about 0.02 s. At this time, SLVs have moved down-

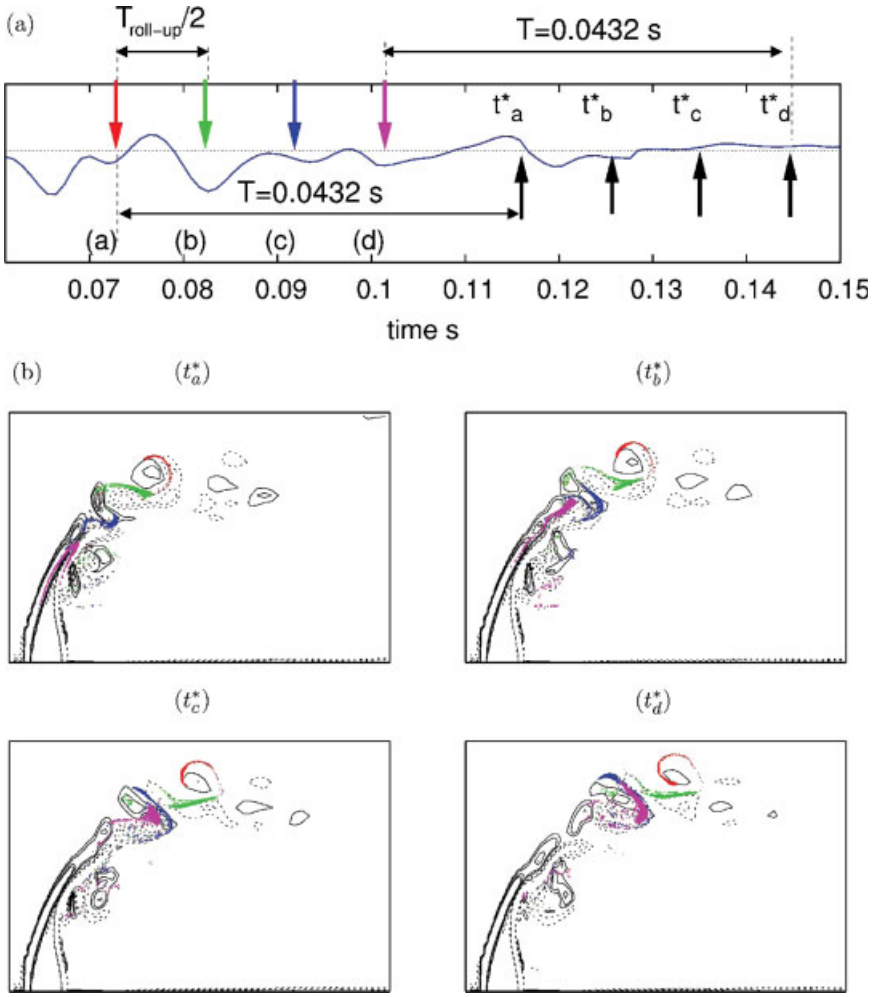

Figure 5. (a) Injection time of four particle packets (colored arrow) and time of visualization (black arrow) and variation of spanwise vorticity (blue line) sampled near the jet exit (sensor 2 of Figure 2) (packets are injected $\Delta T_{roll\text{-}up}/2$ one after the other); (b) snapshot showing particle dispersion 0.0432 s after injection of each packet. Particles from different packets interact with shear layer vortices at a different stage of their evolution.

[Color figure can be viewed in the online issue, which is available at www.interscience.wiley.com.]

stream the jet exit, in the region where we observe the most effective interaction between particles and fluid vortices.

Particle dispersion

We will discuss in details only dispersion results obtained for $D_p = 5$ μm particles, since the response time of these particles is most similar to the time of circulation of shear layer vortices and the maximum interaction between particles and structures is expected. We will focus specifically on the effect produced on particle dispersion by the different time delays of injection. Figure 5 sketches schematically the particle injection times. Time zero (not indicated in the sketch) corresponds to the injection of the first (of 490 simulated) particle packet. Red, green, blue, and purple arrows identify the time of injection of four (out of 490) particle packets chosen for the analysis. These particle packets have been selected among the many others inspected due to their behavior which is relevant to our strategy. The solid line represents the spanwise vorticity signal sampled at sensor 2 of Figure 2. As discussed in Ref. 27, fluctuations associated with the shear layer mode already sensed at the jet exit indicate the initiation of the shear layer instability close to the jet exit. Therefore, a probe located at this point can be used to monitor in real time the formation of SLVs and to adjust the time shift between the pulsed injection of particle and the formation of mixing vortices.

Black arrows identify the time at which the snapshot shown in Figure 5 $(t^*_a) - (t^*_d)$ were taken, that is, a time equal to 0.0432 s after each injection. Injection times for red, green, blue, and purple particles differ by $\Delta T = \Delta T_{roll\text{-}up}/2$ each. This allowed us to evaluate variations in particle dispersion because of the interaction of the four particle packets with a couple of spanwise shear layer vortices at different stages of their evolution.

Figures 5 $(t^*_a) - (t^*_d)$ show four snapshot of particles from packets (a) to (d) 2.27 $\times$ $\Delta T_{roll\text{-}up}$ after the injection of each packet. Only particles contained in the jet symmetry plane (i.e., within the slab $|y/D| < 0.25$) are shown, superposed to spanwise vorticity isocontours, which are used to

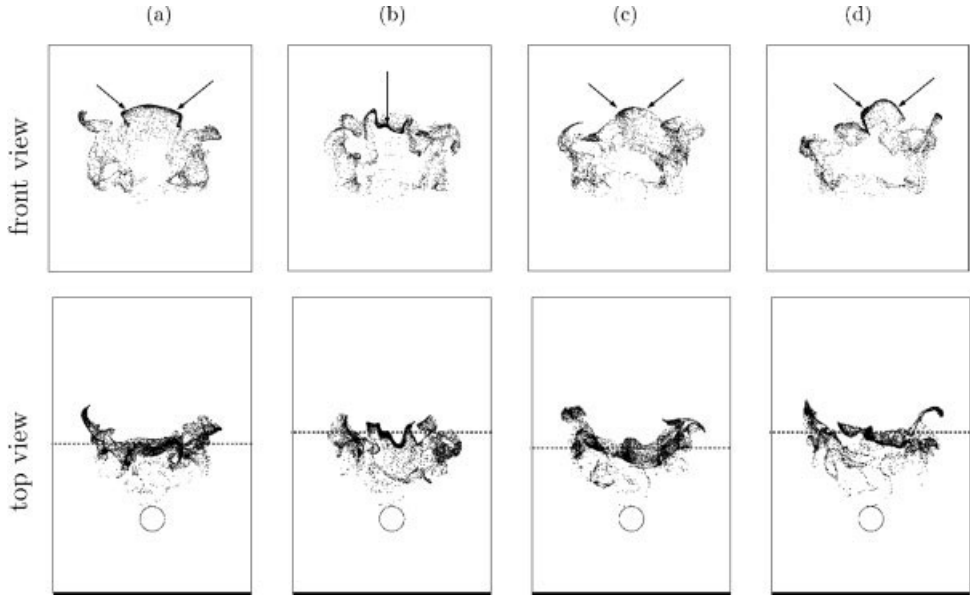

Figure 6. Particle dispersion at time $t^* = 0.043$ s: dispersion patterns are different for packets (a–d).

visualize shear layer vortices. It is clear from the picture that it is rather difficult to find a "regular" sequence of shear layer vortices, corresponding to a regular array of structures when no forcing is used at the jet inlet.

From Figure 5 (t^*_a) and (t^*_c), particles belonging to packets (a) and (c) seem to be effectively entrained by shear layer vortices, being wrapped backward around the vortex in the jet symmetry plane. Particles belonging to packets (b) and (d) seem to escape this strong interaction, moving downstream slightly faster than packets (a) and (c). This of course has consequences on the dispersion of particles, as we will describe in the following Sections.

To evaluate the different tendency of packets to disperse, we considered the dispersion patterns of particle packets after the same time of travel t^* (i.e., after the same time from the injection of each packet). Figure 6 shows the front view and top view of the dispersion pattern of packets (a)–(d) for $t^* = 0.0432$ s. These patterns correspond to snapshots (t^*_a), (t^*_b), (t^*_c), and (t^*_d) of Figure 5, respectively. We observe that the spanwise and radial dispersions are quite different for packets (a)–(d). Front views of particle dispersion (Figure 6, top) show that particles belonging to packet (a) and (c) appear to be lifted up in the region in-between the two arrows. Particles belonging to packet (b) are not lifted up and particles belonging to packet (d) are only partially lifted up. Top views of particle dispersion (Figure 6, bottom) show that, on average, particles belonging to packets (a) and (c) seem to move at a smaller velocity in the streamwise direction. This is made clear by the position of the dashed lines, which identify the streamwise position of the center of mass of each particle packet.

Dispersion and segregation parameters

The specific way in which the interaction between particles and spanwise vortices occurs determines (i) a different advection velocity for particle belonging to different packets, (ii) different radial and streamwise dispersion, and (iii) a different degree of clustering. We tried to quantify these differences in particle dispersion using *ad-hoc* defined dispersion and segregation parameters. First, we tried to quantify differences in advection velocity of particle packets calculating, for each particle packet and for each time step, the distance of the center of mass from the injection point. The convective velocity of each packet is expected to be the same, whichever the time of injection, in a flow in which time dependent vortical structures are absent or play no role in particle dispersion. If time dependent vortical structures exist, they generate local fluctuations in the fluid velocity which can accelerate differently particles belonging to different packets which move in the flow.

Figure 7a shows values calculated for particle packets (a)–(d). The center of mass of particles belonging to packets (b) and (d) moves faster than the center of mass of particles belonging to packets (a) and (c). As shown in Figures 5 and 6, depending on the time of injection, particles either wrap around or remain focused in between spanwise vortices. As a consequence, they are advected downstream with different velocity, experiencing a strong or weak interaction with vortical structures of the flow and being transported into different regions. As expected, pairs of particle packets injected at time instants $\Delta T_{\text{roll-up}}$ apart one from the other show a very similar behavior, confirming that particles interaction with structures is similar if the periodicity for particle injection is tuned to that of structure generation. We quantified the differences in the radial dispersion of particle packets considering the radial distribution of particles with respect to their center of mass at each time step of the dispersion analysis. Specifically, at each time step we calculated (i) the center of mass of the particles, (ii) the three dimensional radial distance of each particle of the packet from its center of mass, and (iii) the frequency distribution of these radial distances. The particle radial distance distribution can be synthetically described using the mean value and the standard deviation of

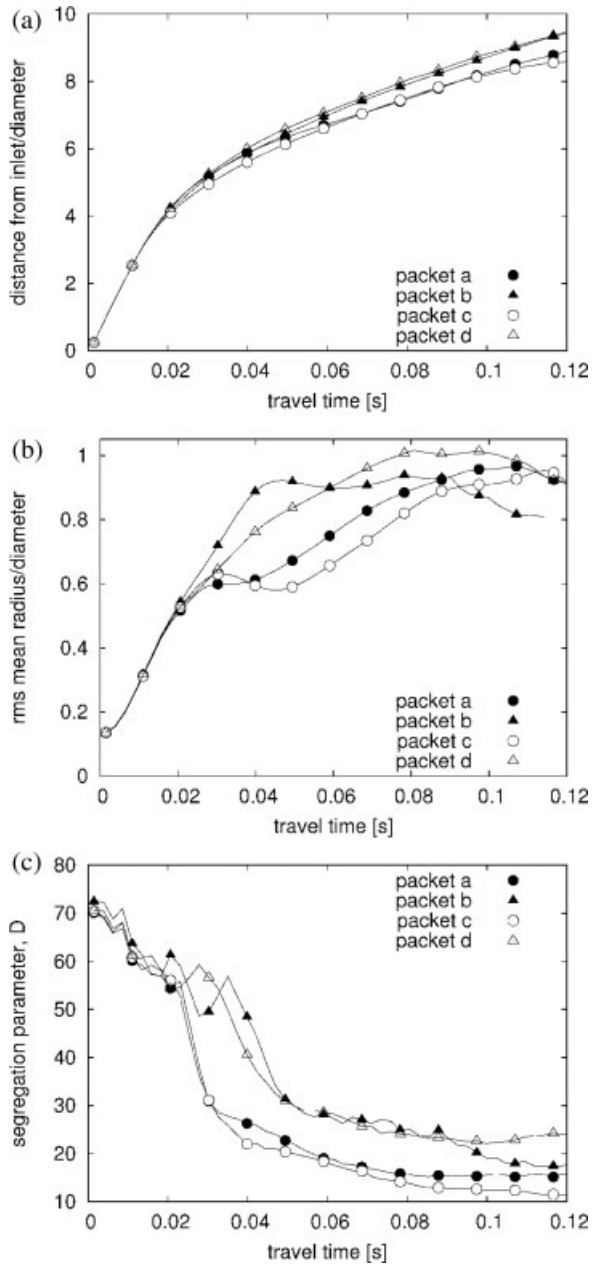

Figure 7. (a) Distance from inlet of particle center of mass for four packets injected $\Delta T_{roll\text{-}up}/2$ one after the other; (b) root mean square variation over time of radial particle distribution for packets (a–d); (c) variation over time of the segregation parameter for packets injected $\Delta T_{roll\text{-}up}/2$ one after the other.

the distribution. If we consider the evolution of a swarm of particles dispersing in an isotropic flow, we expect that the mean value of the radial distance of particles from their center of mass will increase over time, together with the standard deviation of the distribution. If the particles disperse in a flow characterized by large scale vortical structures able to modulate their dispersion, this behavior will be modified. For the particle dispersing in the jet in crossflow, we found that, at each time considered, the mean value of the radial distance (not shown here) does not change significantly for packets (a)–(d), that is, on average the radial spreading of particle packets is independent from the time of injection of the packet. Figure 7b shows the standard deviation of the distribution. This quantity changes significantly among the four packets (a)–(d) after 0.02 s, that is, the time span necessary for the 5 μm particle to cross the shear layer region and to interact with the shear layer vortices. Specifically, packets (b) and (d) exhibit a larger standard deviation in the radial distance distribution, indicating that particles spread less uniformly than packets (a) and (c). This is a first indication of local differences in particle behavior which may be linked to particle entrapment and segregation in specific regions of the flow.

We tried to quantify better the preferential accumulation of particles into specific regions of the flow using the segregation parameter, D, discussed in Ref. 30, which has been used to quantify the degree of organization of particle patterns in homogeneous turbulence[30] and in more complex flow fields, like boundary layers[31] and wakes.[32] The segregation parameter D measures the deviation between the actual distribution of particles and a random distribution, comparing their standard deviations. We should remark here that, differently from the case described by Fessler et al.[30] in the jet in crossflow the random distribution of particles in the whole computational domain does not represent a "realizable" state for the particle/flow system, since (i) the particles are initially clustered at the point of injection and (ii) some regions of the flow (for instance, the region of the crossflow which is upstream the jet orifice) cannot be explored. This poses some interesting issues on the use of D as a robust indicator of particle segregation: the quantifier is biased because the random distribution can not be obtained, and can not discriminate between the clustering generated by injection and the clustering resulting from mixing/demixing by vortical structures. However, these considerations pose no problems to the use of D as indicator of particle segregation since our focus is to identify *differences* among particle packets. The effects of (i) clustering generated by injection and of (ii) the finite dimension of the subdomain which can be explored by the particles are the same for all particle packets. Therefore, differences in packets behavior should definitely be ascribed to the effect of clustering by mixing/demixing vortical structures.

To calculate the particle number distribution, we divided the computational domain into small volumes and we counted the number of particles within each volume. The resulting particle number distribution was then compared with the Poisson distribution, which is the distribution expected when the same number of particles are randomly distributed. The parameter D is calculated as:

$$D = \frac{\sigma - \sigma_{\text{Poisson}}}{\lambda_{\text{Poisson}}} \tag{3}$$

where σ is the standard deviation of the particle number distribution calculated for the transverse jet, σ_{Poisson} is the standard deviation of the Poisson distribution, and λ is the mean number of particles per control volume. A value of $D = 0$ corresponds to a random distribution of particles, $D < 0$

indicates a uniform distribution and $D > 0$ indicates preferential accumulation of particles in specific regions of the flow, that is, segregation. The larger is D, the larger will be the segregation. Since the value calculated for D depends on the size of the box chosen for the analysis, we repeated our calculations for many sizes of the box, choosing for D the maximum value obtained over the different sizes. The length scale corresponding to the maximum value of D allows to discriminate if the clustering is the result of initial segregation or if it is generated by vortical structures. We found that the length scale associated with the maximum value of D increases over time, indicating that while at the starting time clustering is controlled by injection conditions, at later times it is associated with the mixing/demixing action of specific flow structures (SLVs).

Figure 7c shows the evolution over time of the parameter D for particle packets (a)–(d). Initially ($t < 0.02$ s) the value of D is large for all packets indicating the preferential segregation of particles imposed in the issuing volume by injection conditions. This value decreases over time as particles move and disperse into the flow. When the time of flight becomes larger than 0.02 s, that is, precisely when particles interact with shear layer vortices, the values of D start decreasing faster, with a rate of decrease larger for particle packets (a) and (c) than for particle packets (b) and (d). For all packets, the value of D remains very large (in the range 10–25) during the time of travel of particles, indicating that particles do not disperse in the entire volume. Interestingly, after the interaction with shear layer vortices, the value of D for particle packets (a) and (c) becomes lower than for particle packets (b) and (d). This indicates that for packets (a) and (c), the vortical structures are more effective in destroying the initial clustering, dispersing particles more homogeneously in space, whereas for packets (b) and (d), the interaction with the same structures at a different stage of their evolution is not strong enough to promote effective dispersion.

Conclusions

The dispersion of droplets/particles in a transverse stream is the result of the local and instantaneous interaction between the injected species and the large-scale, shear layer vortices (SLVs) populating the transverse jet. In this work, we try to identify strategies based on the pulsed injection of particles to enhance/reduce the particle dispersion in the transverse jet. Specifically, we want to identify the fundamental parameters to monitor to achieve particle dispersion control. The behavior of the particle/flow system is controlled by the periodic evolution of the SLVs, by the probability to have particles where the vortices can entrain them, and by the inertia of particles interacting with the vortices (controlled by the Stokes number). We chose to use a prototypical, simple simulation methodology to prove our strategy, rather than trying to simulate closely the real phenomenon. Despite the assumptions made for the development of the analysis, the model of the transverse jet retains the fundamental characteristics of the flow which have effect on particle dispersion and allows an easier identification of the relevant parameters to monitor to achieve particle dispersion control. We inject particles puffs at the jet mouth synchronizing the injection cycle (characterized by the time period ΔT_{inj}) to the periodicity of formation of the SLVs (characterized by the time period $\Delta T_{roll\text{-}up}$). The particles are injected during a short active period (characterized by duration ΔT_{pulse}) and then move entrained by the jet before interacting with the SLVs, which form a few diameters downstream the jet mouth. Our aim is to establish when the particle cycle should start, with reference to a relevant time which describes the dynamics of the jet in crossflow system, to maximize the entrainment of particles by the SLVs, and thus the interphase mixing.

We made a number of numerical experiments trying to correlate the time of injection of particles with (i) a relevant flow property measured at the jet mouth and with (ii) the dispersion behavior observed. To predict the behavior of the particle/flow system in the perspective of interphase mixing control, we need to develop a low order model of the dispersion process (a black box model) in which the flow property measured at the jet mouth and the dispersion behavior observed, quantified using a proper macroscopic parameter such as D, may represent respectively a state variable and a measure of the system performance. This is a complex task since the interaction between particles and fluid is governed by non linear dynamics. We used a finite volume solver of Navier-Stokes equation to characterize the flow field of the transverse jet and the formation dynamics of shear layer vortices. Then, we used Lagrangian tracking to evaluate the dispersion of particles. Specifically, we considered the effect produced on particle dispersion by a shift in the starting time of the particle injection cycle. We found that (i) when the particle injection cycle has the same period of formation of SLVs, dispersion patterns produced evolve similarly in time, and that (ii) the particle dispersion is maximized for a specific delay in the time of injection. These results indicate that particle pulsed injection can be optimized relative to the cycle of vortical structure generation to enhance/abate dispersion and segregation.

The potentials of this strategy for mixing control are significant: we have shown that the behavior of the particle/flow system can be described in terms of (i) a reduced number of temporal parameters (ΔT_{inj}, ΔT_{pulse}) describing the injection protocol, and by (ii) a time shift which should be tuned basing on (a) a state variable (the spanwise vorticity at the jet mouth) and on (b) one significant performance variable (one of the mixing indicators, like D). The time-shift is indeed the control parameter which can be used effectively to feed-back on the input signal (the pulsed injection) to achieve a given mixing performance with the particle/flow system. Further analysis is required to correlate the size of injected particles with the time delay of injection which ensures the optimal interaction between particles and SLVs and to evaluate the sensitivity of the control strategy to the assumptions made for the development of the model. Specifically, the potential effect of turbulence on particle dispersion control should be evaluated together with the effectiveness of the control strategy on polydispersed swarms of particles. The main modifications expected in a turbulent flow are the following: (i) vortical structures controlling particle dispersion will be smoothed by turbulent diffusion and (ii) segregation of particles into specific regions of the flow will be reduced by turbulent dispersion. Accurate signal processing will be required

to identify the periodical formation of vortices and to find the right time phasing for the injection. Similar effects are expected from the application of the dispersion control strategy to poly dispersed systems. Particle dispersion control will be effective for narrow distribution and less effective for distribution with large spread in particle size. However, we believe that phasing of injection will be still a good choice to control dispersion even for turbulent, poly dispersed jets in crossflow.

Literature Cited

1. Lim TT, New TH, Luo SC. On the development of large-scale structures of a jet normal to a cross flow. *Phys Fluids*. 2001;13:770.
2. Kelso RM, Lim TT, Perry AE. An experimental study of round jets in a cross-flow. *J Fluid Mech*. 1996;306:111–144.
3. New TH, Lim TT, Luo SC. Effects of jet velocity profiles on a round jet in cross-flow. *Exp Fluids*. 2006;40:859–875.
4. Sau A, Hsu TW, Ou SH, Hwang RR. Growth of kidney and antikidney vortices over a square jet in crossflow. *Phys Fluids*. 2006;18: 128102.
5. Shan JW, Dimotakis PE. Reynolds-number effects and anisotropy in transverse-jet mixing. *J Fluid Mech*. 2006;566:47–96.
6. Muppidi S, Mahesh K, Study of trajectories of jets in crossflow using direct numerical simulations. *J Fluid Mech*. 2005;530:81–100.
7. Muppidi S, Mahesh K. Direct numerical simulation of round turbulent jets in crossflow. *J Fluid Mech*. 2007;574:59–84.
8. Campolo M, Degano GM, Soldati S, Cortelezzi L. Influence of inlet conditions on the time-average behavior of transverse jets. *AIAAJ*. 2005;43:1549–1555.
9. Campolo M, Salvetti MV, and Soldati A. Mechanisms for microparticle dispersion in a jet in crossflow. *AIChE J*. 2005;51:28–43.
10. Mungal MG, Lozano A. Some observations of a large, burning jet in crossflow. *Exp Fluids*. 1996;21:264–267.
11. Smith SH, Mungal MG. Mixing, structure and scaling of the jet in crossflow. *J Fluid Mech*. 1998;357:83–122.
12. Eaton JK, Fessler JR. Preferential concentration of particles by turbulence. *Int J Multiphase Flow*. 1994;20:169–209.
13. Shapiro SR, King JM, Karagozian AR, M'Closkey RT. Optimization of controlled jets in crossflow. AIAA-2003–0634, 41st AIAA Aerospace Sciences Meeting and Exhibit, Reno, Nevada, Jan. 6–9, 2003.
14. Karagozian AR, Megerian S, Alves L, George M, Kelly RE. Control of vorticity generation in an acoustically excited jet in crossflow. AIAA-2005–303, 43rd AIAA Aerospace Sciences Meeting and Exhibit, Reno, Nevada, Jan. 10–13, 2005.
15. Fric TF, Roshko A. Vortical structure in the wake of a transverse jet. *J Fluid Mech*. 1994;279:1–47.
16. Kelso RM, Lim TT, Perry AE. New experimental observations of vortical motions in transverse jets. *Phys Fluids*. 1998;10:2427–2429.
17. Kremer DM, Ende MT, Mustakis JG, Ende DJ. A numerical investigation of a jet in an oscillating crossflow. *Phys Fluids*. 2007;19: 095103.
18. Zang Y, Street RL, Koseff JR. A non-staggered grid, fractional step method for time-dependent incompressible Navier-Stokes equations in general curvilinear coordinate systems. *J Comput Phys*. 1994;114: 18–24.
19. Zang Y, Street RL. A composite multigrid method for calculating unsteady incompressible flows in geometrically complex domains. *Int J Num Meth Fluids*. 1995;20:341–350.
20. Rowe PN, Henwood GA. Drag forces in hydraulic model of a fluidized bed. I. *Trans Instn Chem Eng*. 1962;39:43–47.
21. Elgobashi S, Truesdell GC. Direct simulation of particle dispersion in a decaying isotropic turbulence. *J Fluid Mech*. 1992;242:655–700.
22. Yule AJ. Large scale structures in the mixing layer of a round jet. *J Fluid Mech*. 1978;89:413–432.
23. Longmire EK, Eaton JK. Structure of a particle-laden round jet. *J Fluid Mech*. 1992;236:217–257.
24. Sbrizzai F, Verzicco R, Pidria M, Soldati A. Interactions between transitional structures and microparticles in the near-field of a confined turbulent round jet. *Int J Multiphase Flow*. 2004;30:1389–1417.
25. Andreopoulos J. On the structure of jets in a crossflow. *J Fluid Mech*. 1985;157:163–197.
26. Huang RF, Lan J. Characteristic modes and evolution processes of shear layer vortices in an elevated transverse jet. *Phys Fluids*. 2005; 17:034103.
27. Megerian S, Karagozian AR. Evolution of shear layer instabilities in the transverse jet. AIAA-2005–0142, 43rd AIAA Aerospace Sciences Meeting, January 2005.
28. Rudman M. Simulation of the near field of a jet in a cross flow. *Exp Thermal Fluid Sci*. 1996;12:134–141.
29. Camussi R, Guj G, Stella A. Experimental study of a jet in a crossflow at very low Reynolds number. *J Fluid Mech*. 2002;454:113–144.
30. Fessler JR, Kulick JD, Eaton JK. Preferential concentration of heavy particles in a turbulent channel flow. *Phys Fluids*. 1994;6:3742–3749.
31. Picciotto M, Marchioli C, Soldati A. Characterization of near-wall accumulation regions for inertial particles in turbulent boundary layers. *Phys Fluids*. 2005;17:098101.
32. Tang L, Wen F, Yang Y, Crowe CT, Chung JN, Troutt TR. Self-organizing particle dispersion mechanism in a plane wake. *Phys Fluids*. 1992;4:2244–2251.

Manuscript received May 8, 2007, and revision received Apr. 24, 2008.